Geochemistry Geophysics Geosystems G3

Volume 14, Number 3
22 March 2013
doi:10.1029/2012GC004448
ISSN: 1525-2027

Published by AGU and the Geochemical Society

Petrological interpretation of deep crustal intrusive bodies beneath oceanic hotspot provinces

Mark Richards
Department of Earth and Planetary Science, University of California, Berkeley, USA (Mark_Richards@Berkeley.EDU)

Eduardo Contreras-Reyes
Departamento de Geofísica, Universidad de Chile, Santiago, Chile

Carolina Lithgow-Bertelloni
Department of Earth Sciences, University College, London, UK

Mark Ghiorso
OFM Research, Seattle, USA

Lars Stixrude
Department of Earth Sciences, University College, London, UK

[1] Seismic refraction studies of deep-crustal and upper mantle structure beneath some oceanic hotspot provinces reveal the presence of ultramafic bodies with *P*-wave velocities of $Vp \sim 7.4$–8.0 km/s lying at or above the Moho, e.g., Hawaii, the Marquesas, and La Reunion. However, at other hotspot provinces such as the Galapagos, Nazca Ridge, and Louisville the lower crust is intruded by large volumes of gabbroic (mafic) rocks ($Vp \sim 6.8$–7.5 km/s). Ultramafic primary melts formed beneath mature oceanic lithosphere at pressures of ~2–3 GPa (60–90 km depth), and ponded at the Moho due to their relatively high density, can explain the observed ultramafic deep-crustal bodies. By contrast, plume melts formed at depths of ~15–30 km beneath thin lithosphere crystallize assemblages that are more gabbroic. The velocity and density gradient is particularly strong in the pressure range 0.6–1.5 GPa due to the replacement of plagioclase by olivine as melts become more MgO-rich with increasing pressure (and degree) of melting. This anomalous density gradient suggests a possible filtering effect whereby plume melts equilibrated at relatively shallow depths beneath very young and thin oceanic lithosphere may be expected to be of nearly gabbroic (mafic) composition (~6–10% MgO), whereas ultramafic melts (MgO ~ 12–20%) formed beneath older, thicker oceanic lithosphere must pond and undergo extensive olivine and clinopyroxene fractionation before evolving residual magmas of basaltic composition sufficiently buoyant to be erupted at the surface. A survey of well-studied hotspot provinces of highly-varying lithospheric age at the time of emplacement shows that deep-crustal and upper mantle seismic refraction data are consistent with this hypothesis. These results highlight the importance of large-volume intrusive processes in the evolution of hotspot magmas, with intrusive volumes being significantly larger than those of the erupted lavas in most cases. Pyrolite melting can account, to first order, for the total crustal column of magmatic products, whereas alternative models such as selective melting of pyroxenite blobs probably cannot.

Components: 9,200 words, 8 figures, 2 tables.

Keywords: hotspot; seismic refraction; igneous petrology.

Index Terms: 7220 Seismology: Oceanic crust; 8137 Tectonophysics: Hotspots, large igneous provinces, and flood basalt volcanism; 8415 Volcanology: Intra-plate processes (1033, 3615).

Received 20 September 2012; **Revised** 29 November 2012; **Accepted** 30 November 2012; **Published** 22 March 2013.

Richards, M., E. Contreras-Reyes, C. Lithgow-Bertelloni, M. Ghiorso, and L. Stixrude (2013), Petrological interpretation of deep crustal intrusive bodies beneath oceanic hotspot provinces, *Geochem. Geophys. Geosyst.*, *14*, 604–619, doi:10.1029/2012GC004448.

1. Introduction

[2] Seismic imaging of deep crustal structure beneath volcanic edifices and ridges associated with active hotspots such as Hawaii, Marquesas, and Reunion reveal the presence of large bodies of material at the base of the crust with *P*-wave velocities intermediate between normal oceanic lower crustal values and typical mantle values (7.5–8.0 km/s) [*Watts et al*., 1985; *Caress et al*., 1995; *Charvis et al*., 1999]. These bodies are often referred to in terms of ultramafic magmatic "underplating", indicating that they are presumed to contain greater proportions of olivine and pyroxene than normal lower-crustal (gabbroic) rocks in the oceanic crust. The volumes of these ultramafic bodies may be comparable to or greater than the volume of basaltic/gabbroic rocks added to the crust by hotspot activity. Because they occur on otherwise normal oceanic crust and lithosphere, these seismic structures should be diagnostic of the petrological processes associated with hotspot volcanism.

[3] Large-volume ultramafic structures have also been imaged beneath a number of large igneous provinces (LIPs), especially oceanic plateaus such as Ontong-Java, Kerguelen, Agulhas, Manihiki, and Shatsky [*Ridley and Richards*, 2010]. In a previous paper [*Farnetani et al*., 1996], we modeled these structures as intrusive complexes of ultramafic primary melt, gravitationally trapped at the Moho, with perhaps the largest volume fraction representing olivine and clinopyroxene cumulates left behind by cooling and fractionation of the primary mantle melts. Figure 1, adapted from *Farnetani et al*. [1996], illustrates these concepts in relation to the formation of large oceanic plateaus due to the impingement of a mantle plume head upon the oceanic lithosphere.

[4] In this interpretation, the residual melts evolve toward more silicic, lower-density compositions via cooling and crystal fractionation, giving rise to further gabbroic intrusion of the upper crust and basalt extrusion at the surface. This model is valid for melts formed at >10–20 kbars pressure (30–60 km depth), because the mafic content of partial melts derived from mantle pyrolite is known to increase strongly with pressure [*Hirose and Kushiro*, 1993]. Such conditions are obtained for partial melting of hot mantle plume material beneath mature oceanic lithosphere, e.g., the Hawaiian plume undergoing partial melting beneath ~75 Ma age oceanic lithosphere. The mafic contents of magmas also increase with the degree (or temperature) of melting, so that hotter plumes are correspondingly expected to generate more mafic melts.

[5] In this context one might then view each of the hotspot provinces as elegant natural petrological experiments, in which the remnant seismic crustal structures record the various magmatic products whose volume, composition, and evolution are influenced by a number of factors such as the pressure and temperature of melting, initial thickness, composition, state of stress, and density of the crust, initial age of the lithosphere, and the rate of overlying plate motion. Indeed, results from recent high-quality seismic refraction surveys of a number of hotspot provinces reveal widely differing deep crustal seismic structures, e.g., the large ultramafic bodies underlying Hawaii and the Marquesas [*Ten Brink and Brocher*, 1987; *Caress et al*., 1995] vs. the thick but seismically-normal (gabbroic) crust underlying the Cocos Ridge (Galapagos hotspot track) and Iceland [*Sallares et al*., 2003; *Korenaga et al*., 2000]. In this regard, recent imaging of the Louisville Ridge hotspot track suggests unusual deep and shallow crustal intrusive activity [*Contreras-Reyes et al*., 2010] that contrasts markedly with all other hotspots imaged so far.

[6] The diversity of deep crustal structures imaged seismically along active hotspot tracks is illustrated in Figure 2, which shows seismic velocity cross-sections derived from wide-angle refraction studies of structure beneath Hawaii, the Marquesas, Louisville Seamount, and the Cocos Ridge (Galapagos hotspot track). Hawaii and the Marquesas

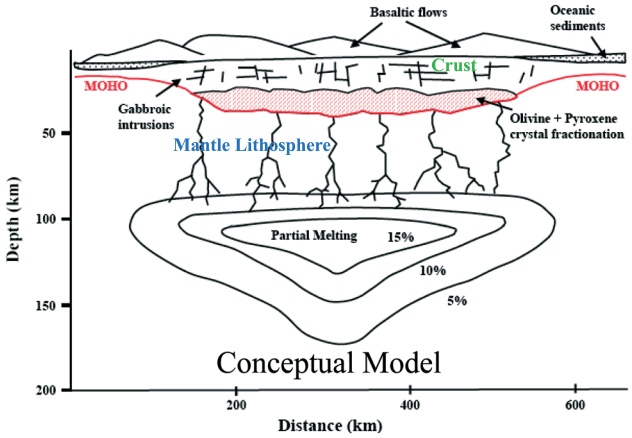

Figure 1. Conceptual model followed in this paper for sublithospheric mantle plume melting, melt migration through the mantle lithosphere, ponding and fractionation of melt at Moho depths (ultramafic), crustal intrusion (mafic), and basalt eruptions (adapted from *Farnetani et al*. [1996]).

both formed on mature oceanic lithosphere, producing conspicuous low-velocity uppermost mantle structures that have been interpreted as ultramafic underplating [*Watts et al*., 1985; *Caress et al*., 1995]. In contrast, the greatly thickened crust underlying the Cocos Ridge, which was produced by the Galapagos plume on effectively zero-age lithosphere at an active spreading center, exhibits seismic velocities consistent with a gabbroic composition to depths as large as ~20 km [*Sallares et al*., 2003]. The case of Louisville Seamount, also emplaced on young (<~10 Ma crust) offers yet another contrast, in that the crust is hardly overthickened at all, and the largely gabbroic intrusions inferred from detailed seismic imaging fill the lower crust and rise to relatively shallow levels within the seamount itself [*Contreras-Reyes et al*., 2010]. Figure 3 from Contreras-Reyes *et al*. [2010] gives a more detailed interpretation of this enigmatic case, in terms of *P*-wave velocity, density structure inferred from simultaneous modeling of seismic structure, gravity, and bathymetry, and a schematic petrological interpretation. We note the presence of a relatively small amount of high-velocity (~7.5 km/s) intrusive material, likely somewhat more mafic than normal gabbro, immediately underlying the Louisville volcano. There are many other examples of imaged crustal structures beneath active hotspot provinces, summarized in Table 2, which we will review later.

[7] In this paper, we seek to explore whether it is possible to discern a consistent influence of the depth of melting (lithospheric age) on the generation of ultramafic intrusive bodies beneath hotspot volcanoes. We use the petrologic modeling codes pMELTS [*Ghiorso et al*., 2002] and HeFESTo [*Stixrude and Lithgow-Bertelloni*, 2005, 2011] to map the influence of depth of melting (pressure) and temperature on the seismic velocities and densities of mantle primary melts and their crystallized products. We then survey deep crustal seismic structures imaged beneath many hotspots over the past several decades, with a focus on the age of the ambient lithosphere at the time of hotspot magmatism, and with a view to discerning the effects of the depth of melting upon the petrological evolution of hotspot magmas. The evidence surveyed appears consistent with the idea that deeper, perhaps hotter, melting beneath older (thicker) lithosphere results in more conspicuous ultramafic intrusive/cumulate bodies formed at Moho depths beneath hotspot volcanoes.

2. Theoretical Models for Sublithospheric Melting and Crystallization Products

2.1. Conceptual Model

[8] Figure 1 gives a conceptual framework for mantle melting, crustal intrusion, and surface eruption due to a mantle plume impinging on mature oceanic lithosphere. A lenticular-shaped melting region forms beneath the lithosphere due to decompression melting of hot, rising plume material. Where sufficiently high melt fractions are obtained, this buoyant primary magma migrates upward via porous flow and/or veining through the overlying lithosphere. Upon encountering the Moho, this magma may become neutrally buoyant (depending upon its composition) and pond as

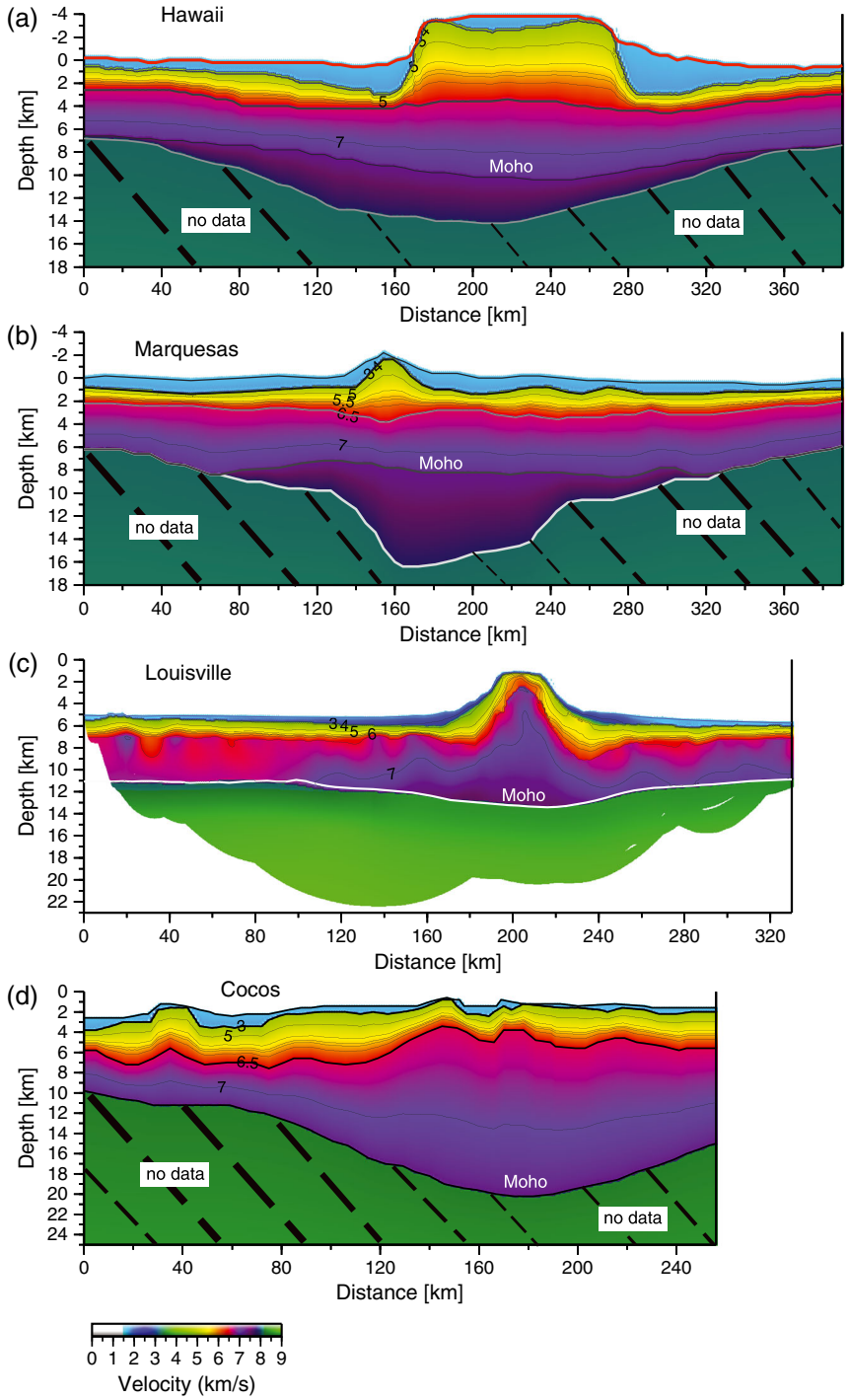

Figure 2. Schematic *P*-wave velocity sections adapted from wide-angle marine refraction studies for Hawaii [*Watts et al.*, 1985], the Marquesas [*Caress et al.*, 1995], the Cocos Ridge (Galapagos hotspot) [*Sallares et al.*, 2003], and Louisville Seamount [*Contreras-Reyes et al.*, 2010].

a gravity current (sill) at the crust-mantle boundary. This ponding is due to the relatively large density contrast between normal overlying oceanic crust of gabbroic composition and normal oceanic mantle. As will be seen in the following sections, for melts produced beneath mature oceanic lithosphere, the primary melts are ultramafic (~15–22% MgO) whose crystallized densities are intermediate between normal mantle and crust values.

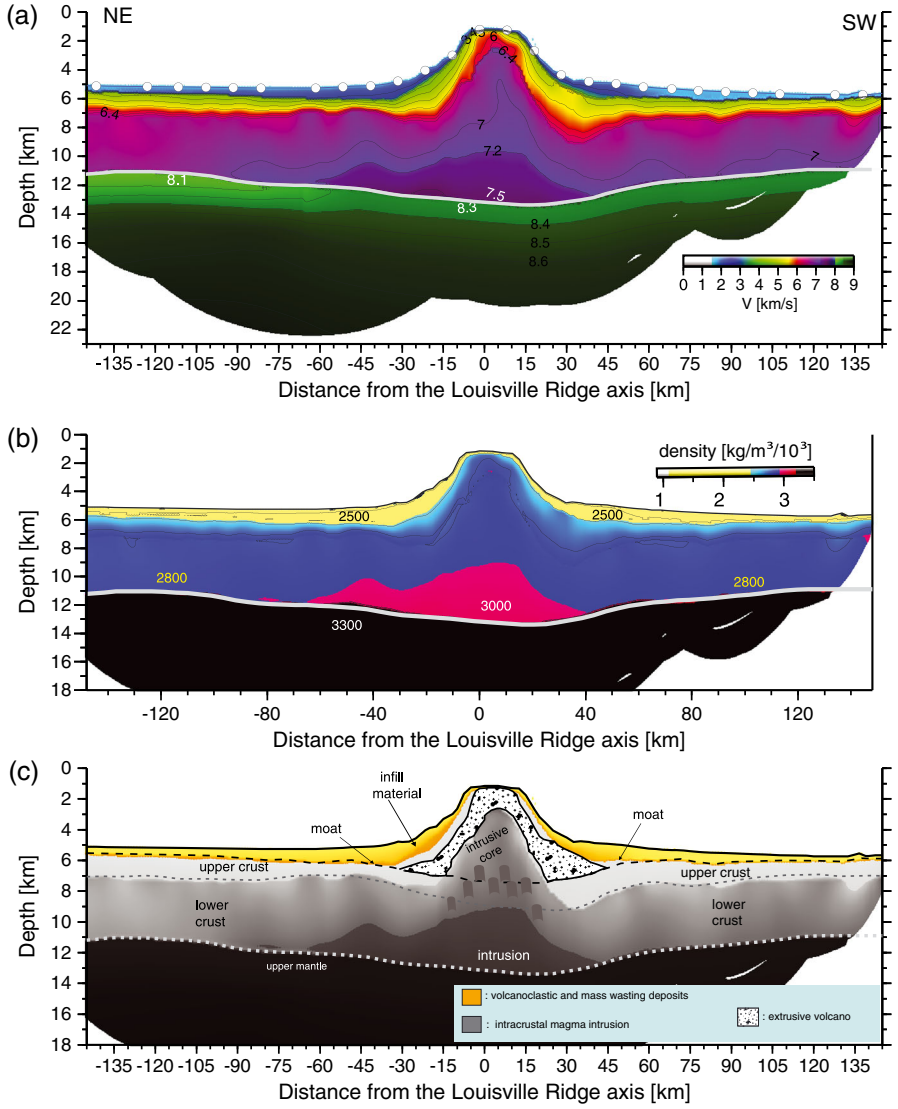

Figure 3. (top) *P*-velocity cross-section, (middle) crustal density model, and (bottom) petrologic interpretation from the seismic study of Louisville Seamount of *Contreras-Reyes et al.* [2010].

[9] For the purposes of this paper we make the crude assumptions that (1) magma leaves the mantle as a "batch" melt, and (2) it rises adiabatically to the Moho. The batch melting assumption is mainly one of convenience, and is contrasted with example results from fractional melting models (Figure 8). In essence, we are assuming that the melt stays in equilibrium with its parent rock (restite), and is then instantaneously removed completely via upward migration. The assumption of adiabatic rise implies that there is no significant interaction, either chemically or thermally, with the intervening lithosphere as the magma rises to the Moho. Although both assumptions are crude, they are commonly employed in modeling hotspot and mid-ocean ridge magmatism, and suffice to illustrate the basic petrological processes of interest.

[10] In a recent paper [*Karlstrom and Richards*, 2011], we have considered the physics of the formation of large magma chambers at the Moho associated with the emplacement of large igneous provinces. Similar processes are invoked here, except that we are interested more in mantle plumes that supply a "steady" source of melt along a hotspot track rather than plume heads generating giant initial eruptions, or flood basalt events. One conclusion of the Karlstrom and Richards study was that these large magma chambers may lead to eruption cycles of duration only ~1 million years, due to the onset of thermally-activated creep and the consequent

shutdown of fracturing processes (dike formation) that are required for surface eruptions. Another finding was that heat loss from these magma chambers and consequent crystal fractionation likely occur rapidly enough to keep up with primary magma injection from the sublithospheric mantle. In other words, the timescale for fractional crystallization is likely short compared to other controls on intrusive/eruptive processes.

[11] Following these basic notions, it is clear that magmas which are initially neutrally-buoyant at the Moho must undergo extensive crystal fractionation of dense (Fe- and Mg-rich) mineral species, in order to become sufficiently buoyant to intrude to shallower levels within and ultimately erupt through the overlying oceanic crust. This process and its consequences for lower-crustal seismic structure beneath hotspot volcanoes is the main focus of this paper.

[12] Referring again to Figure 1, as fractionation of primary magma occurs at the Moho, relatively buoyant mafic magmas rise through the crust forming systems of dikes and sills, ultimately feeding basaltic eruptions at the surface. In this paper we greatly simplify our approach to these processes, and focus on how the composition, density, and seismic velocity of primary melts arriving at the Moho depend upon the depth and temperature of melting in the mantle. The reason for this focus is to aid the interpretation of seismic images of ultramafic bodies (or lack thereof) in the lowermost crust. Figure 4 illustrates the end-member cases to which we refer: deep melting of a hot plume beneath old, thick lithosphere, and shallow melting of a cooler plume beneath young, thin lithosphere. Although seismic imaging may indicate the presence or absence of mafic bodies at shallower levels, the more robust and diagnostic observations are those of deep crustal structures whose seismic velocities are clearly intermediate between normal oceanic crust and mantle, and are therefore less ambiguous in terms of their petrological significance.

[13] In the modeling presented in the next section, we use pMELTS to model the composition of magmas produced by melting of the mantle at various depths and pressures relevant to hotspot magmatism. After obtaining the melt composition we compute the physical properties (density, bulk and shear moduli) of the equivalent frozen material using HeFESTo, a thermodynamic method for calculating phase equilibria and physical properties self-consistently at any pressure and temperature for any composition described by six major oxides (SiO_2, MgO, Al_2O_3, Na_2O, CaO and FeO). This approach allows us to compute the maximum densities and velocities of unfractionated melt upon crystallization at the Moho, and hence an assessment of whether these melt products would be neutrally-buoyant, and what seismic velocities might result. It is important to emphasize that these are indeed minimum density and velocity estimates, as they do not account for subsequent removal of a less dense, lower velocity, gabbroic component to feed shallower intrusions and eruptions.

2.2. Modeling Mantle Melt Compositions

[14] We take a standard approach to modeling the composition of melt produced by batch melting of the mantle in the pressure and temperature ranges of interest. We begin with the standard fertile mantle peridotite composition known as "MM3", which was synthesized for the experiments on mantle melting undertaken by *Baker and Stolper* [1994]. The component oxides of this model mantle material are given in Table 1, where only the limited set of cation species used in our theoretical models are listed.

[15] To model the melting of MM3 we use the thermodynamic code pMELTS (*Ghiorso et al*. [2002]; see http://melts.ofm-research.org/], an improved version of the code MELTS [*Ghiorso and Sack*, 1995; *Asimow and Ghiorso*, 1998]) that includes a much larger experimental database on the thermodynamic equilibrium of silicate systems, and is therefore able to more accurately model the behavior of these systems at pressures as high as 3.5 GPa.

[16] Starting with the MM3 composition, we perform a series of simple theoretical calculations: At a given constant pressure, we begin at a temperature just above the liquidus (100% melt fraction) and cool MM3 through a series of temperature steps, typically about 5–10 °C each, until the limit of accuracy for pMELTS is approached at about 2% melt fraction. At each temperature step pMELTS provides the oxide composition of the melt and solid residuum in equilibrium, i.e., "batch" melts and residuum compositions at a given temperature and pressure. This procedure results in a "map" of equilibrium partial melt component oxide concentrations over the pressure range 0.5–3.5 GPa, and over a range of mantle "potential" temperatures [*McKenzie*, 1984] of ~1500–2000°K. (At any given pressure the temperature range for melt fractions ~0–30% is only of order ~200 °C.)

[17] Figure 5a represents this melt composition mapping in terms of MgO and FeO contents as functions of temperature and degree of melting, with each vertical line of dots corresponding to

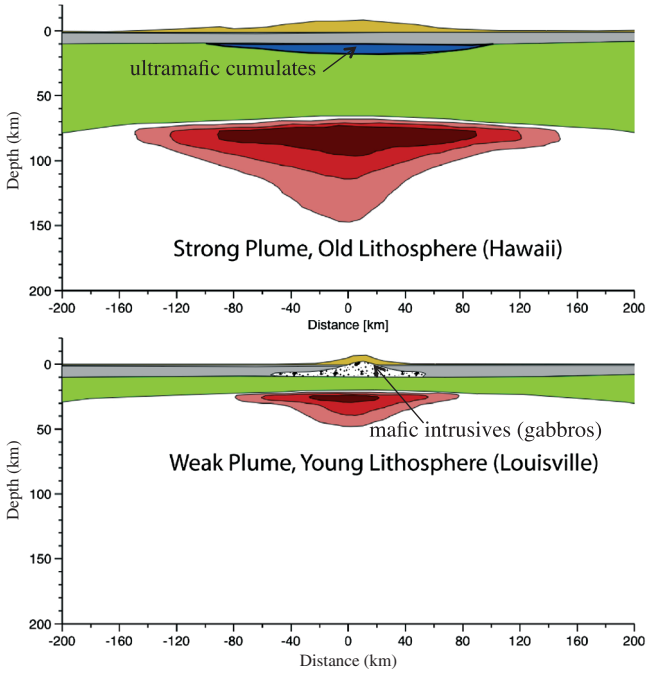

Figure 4. Cartoon contrasting melting and intrusion regimes for deep melting of a hot plume beneath mature lithosphere (top) and shallower melting of a weaker plume beneath younger lithosphere (bottom).

the temperature steps taken within pMELTS at a given pressure. We choose to represent these theoretical calculations in terms of MgO and FeO concentrations because these oxides are important in controlling the resultant seismic velocity and density variations upon crystallization.

[18] Despite the presence of many complicated phase relationships over the temperature and pressure ranges considered, we note the overall simplicity and smoothness of the MgO and FeO variations in Figure 5a. MgO increases monotonically with pressure and melt fraction from values of 8–12% consistent with gabbroic/basaltic compositions at the lowest pressures, to values >15% at pressures >2.0 GPa, corresponding to melting depths beneath mature oceanic lithosphere. This increase in MgO with melting pressure and melt fraction is the most important driver of seismic velocity and density changes in the crystallized melt.

[19] FeO content in the melt also increases monotonically with pressure, but decreases with the degree of melting for pressures less than about 2.0 GPa, in contrast to the behavior of MgO. A plausible explanation for this effect can be inferred from a study of Figure 1 of *Asimow et al*. [2001]. These authors performed some of the first thermodynamic melting calculations on a peridotite composition (reported in *Hart and Zindler* [1986]) using MELTS, the predecessor to pMELTS. Their figure represents a theoretical phase diagram for melt generation to a pressure of 4 GPa. The relevant result from their analysis is that the spacing of calculated melt-fraction isopleths clearly indicates a minimum solidus temperature around 1 GPa. Bulk composition MM3 used in this study with pMELTS translates this minimum to slightly higher pressures. The minimum is characterized by a wide interval of low melt-fraction melting, and since at low-*P* Fe (along with Ti and Na and all the other incompatibles) is always partitioned preferentially over Mg into the liquids, the liquid will have elevated Fe/Mg ratios. The more protracted the interval of melting, the more likely the initial melts will be Fe-rich. The underlying cause for this solidus minimum is that the clinopyroxene (which

Table 1. Pyrolite Model MM3 [*Baker and Stolper*, 1994]

Oxide	wt. %
SiO_2	45.47
TiO_2	0.11
Al_2O_3	4.00
Fe_2O_3	0.68
Cr_2O_3	0.68
FeO	6.61
MgO	38.53
CaO	3.59
Na_2O	0.31

is largely the phase that is melting first) is enriched in Na at pressures above the plagioclase/spinel transition, it being the only major solid phase in the assemblage that readily accommodates the element. Incorporation of Na lowers the stability of clinopyroxene relative to the liquid and hence lowers the solidus temperature. As pressure increases above the minimum melting interval however, the stoichiometry of the melting reaction changes, raising the solidus temperature; since the partial molar volume of Na_2O is higher in the liquid than in the pyroxene, at higher pressures, soda is held in the clinopyroxene preferentially to the liquid and this raises the melting temperature, narrows the melt fraction isopleth spacing, and alters the initial melt composition to be less exotic (less Fe, Ti, Na rich). This effect has been shown experimentally (see *Asimow et al.* [2001] for a discussion). Further increase in pressure diminishes the amount of clinopyroxene in the source assemblage in preference to orthopyroxene, particularly so once garnet is stabilized.

[20] Given that the lowest pressure melts represented in Figure 5a have roughly a basaltic composition (the basic premise of the MM3 composition itself), and given that both density and seismic velocity tend to increase with the MgO and FeO contents of a given silicate liquid/solid composition, these results emphasize the well-known fact that higher pressure melts will crystallize to form mineral assemblages that are of higher density and seismic velocity than gabbros. In the next section we quantify this general statement for the "batch" melt compositions represented in Figure 5a.

2.3. Modeling Primary Melt Crystallization Products

[21] Following our overall conceptual model, we now seek to estimate the densities and seismic velocities of melts that rise to the crust/mantle interface (or above) and crystallize in place. This will allow us to compare the results of petrological modeling to seismological observations, and also to

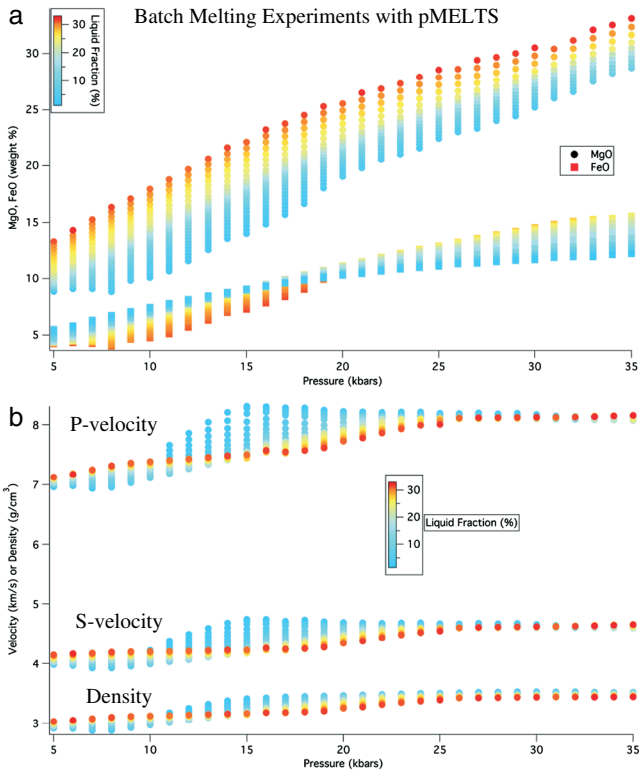

Figure 5. (a) MgO and FeO contents of melts from the pMELTS experiments described in the text. Each vertical column of symbols represents the compositions of residual melts from a model experiment in which an initially completely molten MM3 model mantle composition is held at constant pressure (horizontal axis), while the temperature is lowered incrementally until the liquid is completely solidified. Values are given only in the range 0–30% residual melt fraction. (b) Bulk *P* and *S* wave velocities and densities from the same model experiments for melt products crystallized at 0.3 GPa and 800 °C, as calculated using HeFESTo.

estimate the buoyancy of the crystallized melts relative to the crust and mantle, and hence their likely levels of neutral buoyancy. The pMELTS code does not provide this capability, and instead we rely upon HeFESTo.

[22] HeFESTo, is a thermodynamic, petrologic formalism [*Stixrude and Lithgow-Bertelloni*, 2005, 2011], which enables self-consistent computations of physical properties, phase equilibria, and mantle isentropes. This model uses the concept of fundamental thermodynamic relations [*Callen*, 1960] and Legendre transformations to capture complete information of all equilibrium states in a single functional form. Generalization of the usual isotropic thermodynamics to conditions of anisotropic stress and strain permit self-consistent computation of the full elastic constant tensor, including the bulk and shear moduli, and therefore the longitudinal and shear seismic wave velocities, *VP* and *VS*, respectively. Our calculations consist of three steps. We compute: (1) the equilibrium phase assemblage: the amounts and compositions of coexisting phases by minimizing the Gibbs free energy with respect to the amounts of species at fixed temperature, pressure, and bulk composition, (2) the physical properties of individual phases in the equilibrium assemblage via stress and temperature derivatives of the Gibbs free energy, and (3) the elastic properties of the assemblage as the Voigt-Reuss-Hill average [*Watt et al*., 1976].

[23] Figure 5b gives the results of this thermodynamic modeling of solid phase equilibria for the melt compositions derived from pMELTS, as represented in terms of MgO and FeO contents in Figure 5a. For each melt composition, solid phase equilibrium is calculated at a pressure of 0.3 GPa and a temperature of 800 °C, corresponding roughly to the depth of the oceanic Moho, or slightly deeper, where we expect ultramafic magmas to pond, fractionate, and crystallize. As expected, Figure 5b shows a general increase in seismic velocities and density with pressure of melting (more properly, "last pressure of equilibration" for the melts), although the trends are more complicated than for the MgO and FeO contents alone, due to the appearance of different individual mineral species depending upon composition.

[24] Particularly noteworthy in Figure 5b is that in the pressure range ~0.7–1.5 GPa there is a strong increase in density and velocity at modest melt fractions (<15%), suggesting a strong density filter effect with respect to melting pressure. The reason for this rapid increase is understood straightforwardly in terms of the relation between plagioclase and clinopyroxene/olivine in the crystallized mineral assemblage. Because MgO increases monotonically with pressure of melting (Figure 5a), plagioclase feldspar goes from being the most abundant phase at low pressure to being virtually extinct for melting pressures exceeding about 1.5 GPa. This relationship is illustrated in Figure 6 showing the abundances of major mineral phases in the crystallized melt at Moho depths *vs*. the pressure of melting for total melt fractions of ~10%. The replacement of plagioclase by clinopyroxene and olivine occurs during crystallization mainly over the depth range 0.7–1.5 GPa. Because clinopyroxene and olivine have much higher acoustic velocities and density than plagioclase,

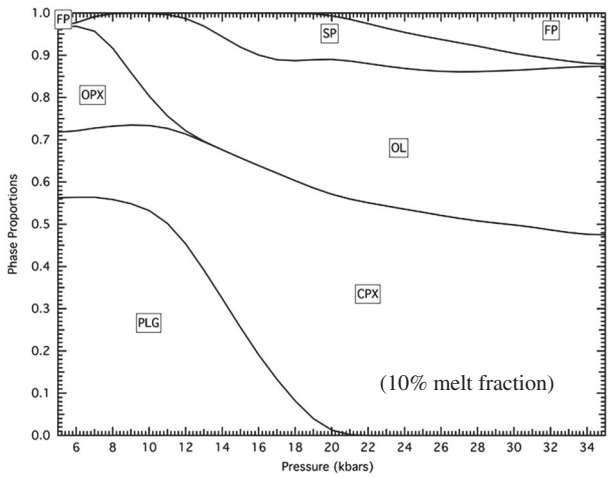

Figure 6. Crystallized mineral phase abundances as a function of melting pressure for initial melt fractions of 10%. (OPX = orthopyroxene, PLG = plagioclase feldspar, SP = spinel, OL = olivine, CPX = clinopyroxene, FP = ferropericlase).

these properties increase rapidly over the same melting pressure range (Figure 5b).

[25] This "phase-aggregate" increase in seismic velocities and density in the restricted range ~0.7–1.5 GPa may have important implications for the behavior of mantle melts derived from different depths of melting. Mantle plumes melting beneath young oceanic lithosphere less than ~20 km thick (~0.8 GPa) will produce magmas that are much more buoyant than for the case of more mature oceanic lithosphere >45 km thick (>1.5 GPa). To be more specific, plume melts from beneath young lithosphere result in crystallized primary melts with densities of order ~2.8–2.9 kg/m^3, comparable to that of gabbros, whereas melts from beneath older lithosphere will result in crystallized densities of >3.0 kg/m^3, which will be trapped between normal gabbroic oceanic lower crust and mantle of density ~3.4 kg/m^3. Thus the former magmas may intrude to form thick crust that is seismically almost indistinguishable from normal lower oceanic crust, whereas the latter may form ultramafic cumulate bodies at the crust/mantle interface. This observation has important implications for the interpretation of deep crustal seismic structure beneath hotspot provinces.

3. Interpreting Seismic Imaging of Deep Crustal Structure at Active Hotspot Tracks

[26] The seismic velocity and density models are represented as contour maps in Figures 7a and 7b, which allow us to suggest the regimes in which the differing crustal sections of Figure 2 may have formed. Again, the basic trends are evident in Figure 7 for increasing density and seismic velocity with increasing pressure and temperature (the latter coupled to degree of melting). A conspicuous feature of Figure 7 is the relatively high sensitivity of velocity and density to increases in pressure compared to increases in temperature through the *P-T* ranges under consideration. In order to produce magmas that could account for the large volume of ultramafic material underlying Hawaii and the Marquesas (Figure 2), pressures of order 20 kbars and potential temperatures of order >100 °C greater than the solidus are required. At the other extreme, production of an anomalously large volume of gabbroic crust at an on-ridge hotspot such as formed the Cocos Ridge (Galapagos hotspot) is consistent with relatively shallow melting and, presumably, relatively modest excess potential temperatures.

[27] A great deal of high-quality seismic refraction work has been done on oceanic hotspot provinces since the publication of *Farnetani et al.*'*s* [1996] hypothesis regarding the origin of ultramafic complexes underlying oceanic plateaus. In Table 2 we present a summary of relevant results from 12 of these hotspot provinces, noting the estimated plate age at the time of hotspot activity, the lowermost crustal *P*-wave velocity, and the presence or absence of ultramafic subcrustal bodies as inferred by the authors (or by us where no inference was drawn). The references for these seismic studies are also listed in Table 2. The provinces listed in Table 2 are organized in order of increasing plate age. Of the first eight provinces, all with inferred ambient plate ages >50 Ma, six show clear seismic evidence for large volumes of underlying ultramafic crustal material lying at the Moho, often described in the literature as "underplating," although we prefer the terms "sill" or "cumulate body" in our interpretation. The Tenerife and Cape Verde provinces appear to lack sufficient seismic resolution beneath the Moho to draw any clear conclusion about the presence or absence of underlying ultramafic bodies [*Watts et al*., 1997; *Wilson et al*., 2010]. It is worth noting that our seismic interpretation is based mainly on seismic velocities and the existence of Moho reflections where they exist. Some seismic experiments recorded reflections from both the prehotspot Moho (PmP) and base of the underplated body or posthotspot Moho reflections, providing better evidence for the presence of underlying ultramafic bodies [*Caress et al*., 1995; *Grevemeyer et al*., 2001]. The lack of posthotspot Moho reflections [e.g., *Watts et al*., 1997; *Contreras-Reyes et al*., 2010] can be interpreted as an indicator of absence of underlying ultramafic bodies.

[28] Four of the remaining five hotspot provinces emplaced upon younger oceanic lithosphere show no clear evidence for ultramafic bodies at the Moho (Louisville, Josephine Seamount, Galapagos, and Iceland). Iceland, with crustal thickness estimates as high as 46 km [*Darbyshire et al*., 1998; *Allen et al*., 2002], is a particularly interesting example, and it is possible that there might be an even deeper body of high-velocity lower crustal cumulate material (R. A. Allen, 2011, personal communication). Iceland, as well as thickened crust at other hotspots, may also be complicated by outward-directed flow of the lower crust [*Jones and Maclennan*, 2005]. The fifth young province, the Ninetyeast Ridge (Kerguelen hotspot), shows clear evidence for large volumes of ultramafic material overlying the Moho at 17°S latitude [*Grevemeyer et al*., 2001]. In this

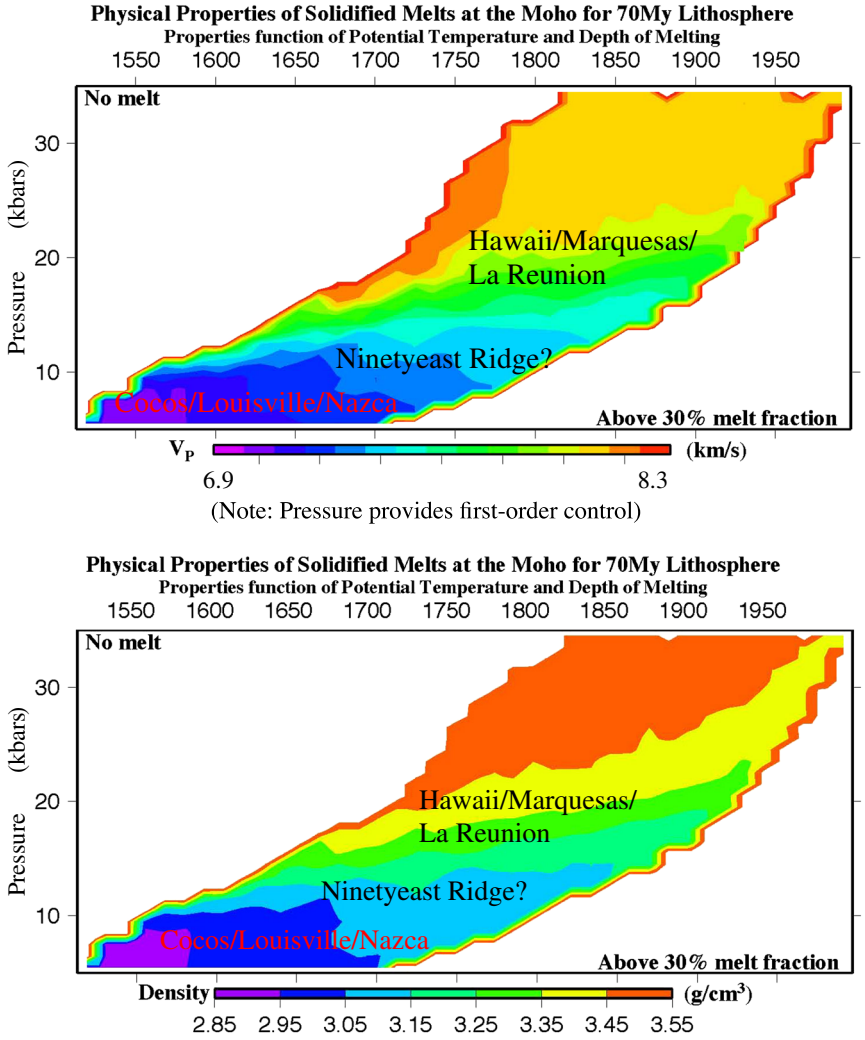

Figure 7. (a) *P*-velocity and density from Figure 5b contoured as a function of melting pressure and (absolute) potential temperature in degrees Kelvin. (b) Density from Figure 5b contoured as a function of melting pressure and (absolute) potential temperature. Possible melting regimes for various hotspots (Hawaii/Marquesas, Ninetyeast Ridge, Cocos/Louisville) are indicated.

case, the constraints on the age of the lithosphere at the time of the emplacement of the Ninetyeast Ridge are weak [*Royer et al.*, 1991], but a reasonable inferred age is ~20 Ma. Although this is a relatively "young" lithospheric age, the inferred thermal thickness of the lithosphere is still of order ~40–60 km, and thus final equilibration pressures for sublithospheric melting will exceed the ~1.5 GPa threshold for melts that will be neutrally buoyant at the oceanic Moho (see Figures 5b and 7). The Nazca Ridge presents a very thick lower crust of 10 km thickness composed of gabbroic rocks and the possible presence of intrusions in the lowermost crust with seismic velocities falling in the range 6.7–7.5 km/s [*Hampel et al.*, 2004]. This oceanic ridge was formed at the Easter Island hotspot on the Pacific-Farallon/Nazca spreading center [*Pilger*, 1984].

[29] A recent seismic survey was conducted along the Marcus-Wake seamount chain [*Kaneda et al.*, 2010], where its associated volcanic edifice was emplaced on a super plume environment in the northwest Pacific basin. Their main results are high-velocity, intrusive cores at shallow depths and low upper mantle velocities (7.5–8.0 km/s). The authors did not attribute low upper mantle velocities to ultramafic bodies at the Moho, but instead they interpreted these features as sill-like intrusion of rising fractionated magma from the

Table 2. Seismic Results from Oceanic Hotspots

Hotspot Province	Plate Age (Ma)	Lower Crust Velocity (km/s)	Ultramafic Subcrustal Body? (Velocity [km/s])	References	Comments
Tenerife	120	7.0–7.2	???	[*Watts et al*., 1997]	Poor mantle resolution
Gran Canaria	80–120	6.6–7.3	Yes (7.4–7.8)	[*Ye et al*., 1999]	
Cape Verde	> 110	7.0–7.3	???	[*Wilson et al*., 2010]	No direct evidence for subcrustal body
Super Meteor	70	7.0–7.5	Yes (7.5–8.0)	[*Weigel and Grevemeyer*, 1999]	
Hawaii	60–80	6.5–6.9	Yes (7.4–7.8)	[*Watts et al*., 1985; *Watts and Ten Brick*, 1989]	
La Reunion	62	6.4–7.0	Yes (~7.5)	[*Charvis et al*., 1999]	
Marquesas	~57	6.5–7.5	Yes (7.6–8.0)	[*Caress et al*., 1995]	
Ninetyeast	~20 ???	~7.2	Yes (7.5–8.0)	[*Grevemeyer et al*, 2001]	
Louisville	<10	7.2–7.5	No	[*Contreras-Reyes et al*., 2010]	
Josephine Seamount	0	6.4–6.8	???	[*Pierce and Barton*, 1991]	Unconstrained Moho
Galapagos (Cocos and Malpelo)	0	7.0–7.1	No	[*Sallares et al*., 2003]	Very thick normal velocity crust (20–30 km); no upper mantle resolution
Iceland	0	7.0–7.2	No?	[*Korenaga et al*., 2000; *Darbyshire et al*., 2000; *Allen et al*., 2002]	Very thick normal velocity crust (~30 km); no upper mantle resolution
Nazca	0	6.5–7.5	No?	[*Hampel et al*., 2004]	Very thick normal velocity crust (~14 km)

mantle [*Farnetani et al*., 1996]. In addition, high-velocity structures at seamount centers (>6.0 km/s), usually interpreted as intrusive cores, have been found in La Reunion [*Gallart et al*., 1999; *Charvis et al*., 1999], Great Meteor Seamount [*Weigel and Grevemeyer*, 1999], Hawaii [*Zucca et al*., 1982], and Louisville [*Contreras-Reyes et al*., 2010].

[30] Summarizing the results of Table 2, where sufficient seismic resolution exists, data from the 14 provinces listed support our hypothesis that older ambient lithosphere, and hence greater depth of last melt equilibration with the parent mantle rocks, results in primary melts reaching the base of the crust that are much more Fe and Mg rich, giving densities and seismic velocities that are intermediate between those of normal oceanic crust and mantle. The data from Tenerife, Cape Verde, and Josephine are inconclusive, and thus do not present counter-examples. Better constraints on lithospheric age at the time of the emplacement of the seismically-imaged section of the Ninetyeast Ridge [*Grevemeyer et al*., 2001] would greatly aid in the interpretation of this important example.

4. Discussion

[31] Other authors have used petrological models to explain the deep crustal structure of hotspot provinces formed in near-ridge environments, e.g., the Iceland/North Atlantic system [*Korenaga et al*., 2002] and the Galapagos/Cocos Ridge system [*Sallares et al*., 2005]. Their interpretations of crustal structure are consistent with the models we have presented here, and our work extends this type of analysis to hotspots that occur on more mature oceanic lithosphere and involve greater effective melting pressures, emphasizing the role of crystal fractionation in forming high-velocity bodies at the crust-mantle interface.

[32] Large high-velocity bodies in the deep crust have also been known for some time to occur beneath large igneous provinces (LIPs) [e.g., *Furumoto et al*., 1976; *White et al*, 1987] that occur at the initiation of hotspots [*Richards et al*., 1989; *Coffin et al*., 2006]. *White et al*. [2008] imaged large volumes of mafic intrusions, as opposed to sub-Moho "underplating," at the Faroe and Hatton Bank volcanic margins (ocean-continent transition) in the North Atlantic

(Iceland) province, consistent with the findings of *Hopper et al*. [2003] along the SE Greenland volcanic margin. For LIPs, relating lithospheric emplacement age (thickness) to melting pressure is perhaps less straightforward, since these massive events are disruptive of the ambient lithosphere. We recently reviewed the deep seismic structure of LIPs globally [*Ridley and Richards*, 2010], and found extensive evidence for large-volume ultramafic bodies emplaced at Moho depths beneath most oceanic LIPs, consistent overall with the models of *Farnetani et al*. [1996] for the enormous Ontong-Java Plateau and of *Korenaga et al*. [2005] for the North Atlantic province

[33] Various geochemical data can be used to infer variations in melting depth, e.g., inversion of trace and rare earth element abundances [*McKenzie and O'Nions*, 1991]. *Ellam* [1992] found that Ce/Y and Ce/Yb ratios increased systematically with increasing lithospheric age (thickness) for oceanic hotspot provinces, indicating a corresponding increase in melting depth that is consistent with our results. *Fram and Lesher* [1993] studied both major- and trace-element variations in the North Atlantic tertiary province, and inferred decreasing melting depth as the continental lithosphere thinned progressively with the opening of the ocean basin. Although not attempted here, a more comprehensive study of combined geochemical and seismological constraints involving both major and minor element behavior would seem a promising avenue for further work.

[34] The data from seismic surveys in Table 2 are consistent with the hypothesis of melting-depth as a control on the formation of ultramafic bodies at the Moho beneath hotspot volcanoes. However, the models we have developed remain crude, and largely petrological, in nature. We believe we have made a strong plausibility argument, but models that connect the movement and evolution of melt thermodynamically with mantle convection and melt extraction/migration processes are obviously needed to provide a more sophisticated interpretation of the seismic data and their relation to volcanic products at the surface.

[35] A first-order improvement to our work would be incorporation of the pMELTS petrological model into a thermal convection model for mantle plume melting beneath the lithosphere, as done for Hawaii by *Watson and McKenzie* [1991] using the *McKenzie and Bickle* [1988] parameterization of mantle melting. In this regard, we note that the compositions of primary melts derived by *Watson and McKenzie* [1990] are consistent with our model inferences here, but they did not connect this result to the discovery of the very large ultramafic body seismically-imaged beneath the Hawaiian chain by *Watts and ten Brink* [1989].

[36] An even greater limitation of most published models for hotspot melting is the assumption of batch melting. Therefore, a zeroeth-order modeling consideration is that of fractional melt extraction. Figure 8 shows results from a simple experiment on batch vs. fractional melting using pMELTS: We compute fractional and batch melting results beginning with a common P,T condition for the onset of partial melting at 20 kbars. For batch melting, we proceed to reduce the pressure and compute the melt products in equilibrium with the residuum as before. For fractional melting, we reduce the pressure by steps of 2 kbars at a time, extracting the melt at each step and "storing" it to keep track of the average melt composition as pressure is reduced to 10 Kbars. Figure 8 shows the MgO weight fraction in the melt for both experiments as a result of the final pressure. Fractional melting has a modest effect upon the major-element composition of the average melt products, i.e., up to a maximum ~15% increase in MgO in the melt. This increase, of course, leads to further reduction in the fraction of plagioclase present in the final crystallized melt product at Moho pressures, and thus only

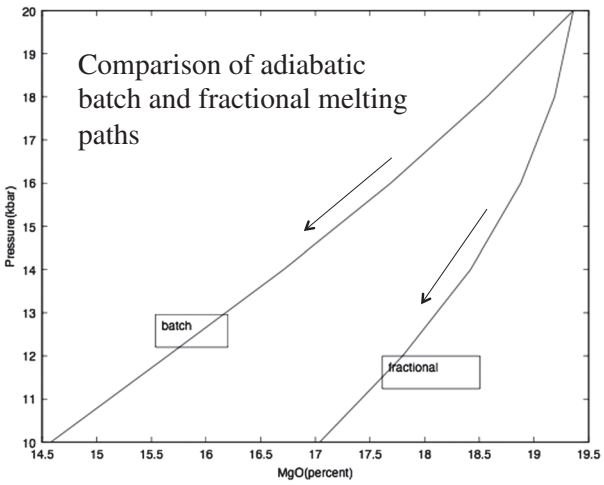

Figure 8. Comparison of MgO content of residual melt as a function of melting pressure (vertical axis) for adiabatic batch and fractional melting experiments using pMELTS, starting from a common initial state that just encounters the solidus (initial melting) at 20 kbars. For the fractional melting curve, melt is "removed" at 2 kbar intervals and "stored" to compute a running average composition for total melt extracted as a function of pressure.

strengthens the density filter effect that stands at the core of our overall hypothesis.

[37] We have assumed a canonical pyrolite composition for the major element composition of the mantle, which strongly determines the outcomes of the thermodynamic experiments represented in Figures 5–8. Alternative models for mantle plume melting to produce hotspots include melting of trace-element-enriched pyroxenite blobs embedded in more pyrolitic mantle [e.g., *Ito and Mahoney*, 2005a, 2005b; *Sobolev et al*., 2007; *Bianco et al*., 2011]. An advantage of such a model is that it might explain the distinct trace-element and isotopic signatures of some hotspots without invoking physically distinct geochemical reservoirs in the mantle. Instead, the pyroxenite blobs are considered to be mechanically-mixed into an ambient depleted mantle, and are able to undergo partial melting at higher (sublithospheric) pressures, thus dominating the trace element signatures of hotspot lavas. Aside from the problem of maintaining chemical disequilibrium between this enriched partial melt and the ambient mantle through which it must migrate upward before being emplaced in the crust, the seismic results we have summarized here point to another problem with this type of model: Partial melting of pyroxenite cannot account for primary magmas with FeO and MgO contents that are sufficiently high to explain Moho-level ultramafic intrusive bodies whose volumes are comparable to or greater than those of the erupted basalts and intruded midcrustal gabbros. (The deep instrusive bodies are most likely of roughly pyroxenitic composition themselves, and partial melting of pyroxenite does not yield pyroxenite.) Thus the presence of large-volume, high-velocity intrusive bodies beneath hotspots would appear consistent with pyrolite melting models for mantle plumes, but not with the notion of plume magmas being dominated by partial melting of ubiquitous blobs of pyroxenite.

5. Conclusions

[38] Evidence from seismic imaging of the crust and uppermost mantle beneath hotspot tracks shows that high-velocity (ultramafic) intrusive bodies at the crust/mantle interface are a ubiquitous feature of hotspot magmatism formed at mature oceanic lithosphere. By contrast, the seismic evidence indicates that thickened crust at hotspot tracks formed in near-ridge (thin lithosphere) environments is largely gabbroic in composition. These observations are straightforwardly understood in terms of pyrolite melting models, wherein higher pressure melting beneath mature lithosphere generates ultramafic primary melts that must undergo extensive crystal fractionation at a density trap in the lowermost crust before leading to largely basaltic eruptions at the surface. For effectively zero-age ambient lithosphere, the melt products are, naturally, similar to the basaltic/gabbroic compositions of mid-ocean ridges that are produced in lower pressure melting environments. The fact that the bulk of hostpot lavas are basaltic in composition is thus primarily a consequence of the Moho density filter formed at normal mid-ocean ridges, with the necessary fractionation of primarily olivine and pyroxene for mature lithospheric environments evident in the deep crustal high-velocity bodies imaged beneath hotspots such as Hawaii, Marquesas, and La Reunion. An important modeling result is the discovery of an anomalously steep increase in the seismic velocity and density of crystallized melt products as melting pressure increases through the critical range of 0.6–1.5 GPa, implying a strong filtering process on primary melt composition as the oceanic lithosphere increases in thickness from ~20–40 km. An alternative hotspot model that invokes melting of ubiquitous pyroxenitic blobs does not offer an obvious explanation for the seismic observations we have summarized.

Acknowledgments

[39] We gratefully acknowledge comments and reviews from Ingo Grevemeyer, Sally Gibson, an anonymous reviewer, and editor Thorsten Becker. This work was supported in part by a grant to MR by the National Science Foundation.

References

Allen, R. M., et al. (2002), Plume-driven plumbing and crustal formation in Iceland, *J. Geophys. Res.*, *107*, 2163, doi:10.1029/2001JB000584.

Asimow, P. D., and M. S. Ghiorso (1998), Algorithmic modifications extending MELTS to calculate subsolidus phase relations, *Am Mineralogist*, *83*, 1127–1131.

Asimow, P. D., M. M. Hirschmann, and E.M. Stolper (2001), Calculation of peridotite partial melting from thermodynamic models of minerals and melts: IV. Adiabatic decompression and the composition and mean properties of mid-ocean ridge basalts, *J. Petrology*, *42*, 963–998.

Baker, M. B., and E. M. Stolper (1994), Determining the composition of high-pressure mantle melts using diamond aggregates, *Geochim. Cosmochim. Acta*, *58*, 2811–2827.

Bianco, T. A., G. Ito, J. van Hunen, M. D. Ballmer, and J. J. Mahoney (2011), Geochemical variations at intraplate hot spots caused by variable melting of a veined mantle plume, *Geochem., Geophys, and Geosys*, *12*, Q0AC13.

Callen, H. G. (1960), *An Introduction to the Physical Theories of Equilbrium Thermostatics and Irreversible Thermodynamics*, Wiley, New York, 376 pp.

Caress, D. W., M. K. McNutt, R. S. Detrick, and J. C. Mutter (1995), Seismic imaging of hotspot-related crustal underplating beneath the Marquesas Islands, *Nature*, *373*, 600–603.

Charvis, P., et al. (1999), Spatial distribution of hotspot material added to the lithosphere under La Reunion from wide-angle seismic data, *J. Geophys. Res.*, *104* doi: 10.1029/98JB02841.

Contreras-Reyes, E., I. Grevemeyer, A. B., Watts, L. Planert, E.R. Flueh, and C. Pierce (2010), Crustal intrusion beneath the Louisville hotspot track, (289), 323-333, *Earth Planet. Sci. Lett.*, doi:10.1016/j.epsl.2009.11.020.

Coffin, M. F., R. A. Duncan, O. Eldholm, J. G. Fitton, F. A. Frey, H. C. Larsen, J. J. Mahoney, A. D. Saunders, R. Schlich, and P. J. Wallace (2006), Large Igneous Provinces and Scientific Ocean Drilling: Status Quo and A Look Ahead, *Oceanography*, *19*, 150–160.

Darbyshire, F. A., I. T. Bjarnason, R. S. White, and O. G. Flovenz (1998), Crustal structure above the Iceland mantle plume imaged by the ICEMELT refraction profile, *Geophys. J. Int.*, *135*, 1131–1149.

Ellam, R. M. (1992), Lithospheric thicknes as a control on basalt geochemistry, *Geology*, *20*, 153–156.

Farnetani, C., M. Richards, and M. Ghiorso (1996), Petrological models of magma evolution and deep crustal structure beneath hotspots and flood basalt provinces, *Earth Planet. Sci. Lett.*, *143*, 81–94.

Fram, M. S., and C. E. Lesher (1993), Geochemical constraints on mantle melting during creation of the North Atlantic basin, *Nature*, *363*, 712–715.

Furumoto, A. S., J. P. Webb, M. E. Odegard, and D. M. Hussong (1976), Seismic studies on the Ontong Java Plateau, *Tectonophysics*, *34*, 71–90.

Gallart, J., L. Driad, P. Charvis, M. Sapin, A. Hirn, J. Diaz, B. de Voogd, and M. Sachpazi (1999), Perturbation to the lithosphere along the hotspot track of La Réunion from an offshore-onshore seismic transect, *J. Geophys. Res.*, *104* (B2), 2895–2908.

Ghiorso, M. S., M. M. Hirschmann, P. W. Reiners, and V. C. Kress, III (2002), The pMELTS: A revision of MELTS for improved calculation of phase relations and major element partitioning related to partial melting of the mantle to 3 GPa, *Geochem, Geophys, Geosys*, *3*, doi:10.1029/2001GC000217.

Ghiorso, M. S., and R. O. Sack (1995), Chemical mass transfer in magmatic processes IV: A revised and internally consistent thermodynamic mondel for the interpolation and extrapolation of liquid-solid equilibria in magmatic systems at elevated temperatures and pressures, *Contrib. Min. Petrol.*, *119*, 197–212.

Grevemeyer, I., E. R. Flueh, C. Reichert, J. Bialas, D. Klaschen, and C. Kopp (2001), Crustal architecture and deep structure of the Ninetyeast Ridge hotspot trail from active-source ocean-bottom seismology, *Geophys. J. Int.*, *144*, 414–431.

Hampel, A., N. Kukowski, J. Bialas, C. Huebscher, and R. Heinbockel (2004), Ridge subduction at an erosive margin: The collision zone of the Nazca Ridge in southern Peru, *J. Geophys. Res.*, *109*, B02101, doi:10.1029/2003JB002593.

Hart, S. R., and A. Zindler (1986), In search of a bulk-Earth composition, *Chem. Geol.*, *57*, 247–267.

Hirose, K., and I. Kushiro (1993), Partial melting of dry peridotites at high pressures: Determination of compositions of melts segregated from peridotite using aggregates of diamond, *Earth Planet. Sci. Lett.*, *114*, 477–489.

Hopper, J. R., T. Dahl-Jensen, W. S. Holbrook, H. C. Larsen, D. Lizarralde, J. Korenaga, G. M. Kent, and P. B. Kelemen (2003), Structure of the SE Greenland margin from seismic reflection and refraction data: Implications for nascent spreading center subsidence and asymmetric crustal accretion during North Atlantic opening, *J. Geophys. Res.*, *108*, 2269, doi:10.1029/2002/B001996.

Ito, G., and J. J. Mahoney (2005a), Flow and melting of a heterogeneous mantle: 1. Method and importance to the geochemistry of ocean island and mid-ocean ridge basalts, *Earth Planet. Sci. Lett*, *230*, 29–46.

Ito, G., and J. J. Mahoney (2005b), Flow and melting of a heterogeneous mantle: 2. Implications for a chemically nonlayered mantle, *Earth Planet. Sci. Lett*, *230*, 47–63.

Jones, S. M., and J. Maclennan (2005), Crustal flow beneath Iceland, *J. Geophys. Res.*, *110*, B09410.

Kaneda, K., S. Kodaira, A. Hishizawa, T. Morishita, and N. Takahashi (2010), Structural evolution of preexisting oceanic crust through intraplate igneous activities in the Marcus-Wake seamount chain, *Geochem, Geophys, and Geosys*, *11*, doi:10.1029/2010GC003231.

Karlstrom, L., and M. A. Richards (2011), On the evolution of large ultramafic magma chambers, or sills, and timescales for flood basalt eruptions, *J. Geophys. Res.*, *116*, B08216.

Korenaga, J., W. S. Holbrook, G. M. Kent, P. B. Kelemen, R. S. Detrick, H. C. Larsen, J. R. Hopper, and T. Dahl-Jensen (2000), Crustal structure of the southeast Greenland margin from joint refraction and reflection seismic tomography, *J. Geophys. Res.*, *105*, 21591–21614.

Korenaga, J., P. B. Kelemen, and W. S. Holbrook (2002), Methods for resolving the origin of large igneous provinces from crustal seismology, *J. Geophys. Res.*, *107*, 2178, doi:10.1029/2001JB001030.

McKenzie, D. P. (1984), The generation and compaction of partially molten rock, *J. Petrology*, *25*, 713–765.

McKenzie, D. P., and M. J. Bickle (1988), The volume and composition of melt generated by extension of the lithosphere, *J. Petrology*, *29*, 625–679.

McKenzie, D. P., and R. K. O'Nions (1991), Partial melt distributions from inversion of rare earth element concentrations, *J. Petrol.*, *29*, 625–679.

Pierce, C., and P. Barton (1991), Crustal structure of the Madeira-Tore Rise, eastern North Atlantic – results of a DOBS wide-angle and normal incidence seismic experiment in the Josephine Seamount region, *Geophys. J. Int.*, *106*, 257–378.

Pilger, R. H. (1984), Cenozoic plate kinematics, subduction and magmatism, South American Andes. *J. Geol. Soc. Lond. 141*, 793–802.

Richards, M. A., R. A. Duncan, and V. Courtillot (1989), Flood basalts and hotspot tracks: Plume heads and tails, *Science*, *246*, 103–107.

Ridley, V. A., and M. A. Richards (2010), Deep crustal structure beneath large igneous provinces and the petrologic evolution of flood basalts, *Geochem. Geophys. Geosyst.*, *11*, Q09006.

Royer, J.-Y., J. W. Peirce, and J. K. Weissel (1991), Tectonic constraints on the hot-spot formation of Ninetyeast Ridge, in *Proc. ODP Sci. Results*, edited by J. K. Weissel, *et al.*, 121, 763–776, Ocean Drilling Program, College Station, TX.

Sallarès, V., P. Charvis, E. R. Flueh, and J. Bialas (2003), Seismic structure of Cocos and Malpelo Volcanic Ridges and implications for hot spot-ridge interaction, *J. Geophys. Res.*, *108*(B12), 2564, doi:10.1029/2003JB002431.

Sallarès, V., P. Charvis, E. R. Flueh, and J. Bialas and the SALIERI Scientific Party (2005), Seismic structure of the Carnegie ridge and the nature of the Galapagos hotspot, *Geophys. J. Int.*, *161*, 763–788.

Sobolev, A. V., et al. (2007), The amount of recycled crust in sources of mantle-derived melts, *Science*, *316*, 412–417.

Stixrude, L., and C. Lithgow-Bertelloni (2005), Mineralogy and elasticity of the oceanic upper mantle: Origin of the low velocity zone, *J. Geophys. Res.*, *110*, B03204, doi: 10.1029/2004JB002965.

Stixrude, L., and C. Lithgow-Bertelloni (2011), Thermodynamics of mantle minerals II, Phase equilibria, *Geophys. J. Int.*, *184*, 1180–1213.

ten Brink, U. S., and T. M. Brocher (1987), Multichannel seismic evidence for a subcrustal intrusive complex under Oahu and a model for Hawaiian volcanism, *J. Geophys. Res.*, *92*, 13687–13707.

Watson, S., and D. McKenzie (1991), Melt generation by plumes: A study of Hawaiian volcanism, *J. Petrolology*, *32*, 501–537.

Watt, J. P., G. F. Davies, and R. J. O'Connell (1976), The elastic properties of composite materials, *Rev. Geoph. Spac. Phys.*, *50*, 6290–6295.

Watts, A. B., and U. S. Ten Brink (1989), Crustal structure, flexure, and subsidence history of the Hawaiian islands, *J. Geophys. Res.*, *94*, 10473–10500.

Watts, A. B., U. S. ten Brink, P. Buhl, and T. Brocher (1985), A multichannel seismic study of lithospheric flexure across the Hawaiian-Emperor seamount chain, *Nature*, *315*, 105–111.

Watts, A. B., C. Pierce, J. Collier, R. Dalwood, J. P. Canales, and T. J. Henstock (1997), A seismic study of lithosphere flexure in the vicinity of Tenerife, Canary Islands, *Earth Planet Sci. Lett.*, *146*, 431–447.

Weigel, W., and I. Grevemeyer (1999), The Great Meteor seamount: Seismic structure of a submerged intraplate volcano, *J. Geodyn.*, *28*, 27–40.

White, R. S., L. K. Smith, A. W. Roberts, P. A. F. Christie, N. J. Kusznir, and the iSIMM Team (2008), Lower-crustal intrusion on the North Atlantic continental margin, *Nature*, *452*, 460–464.

White, R. S., G. D. Spence, S. R. Fowler, D. P. McKenzie, G. K Westbrook, and A. N. Bowen (1987), Magmatism at rifted continental margins, *Nature*, *330*, 439–444.

Wilson, D. J., C. Peirce, A. B. Watts, I. Grevemeyer, and A. Krabbenhoeft (2010), Uplift at lithospheric swells – I: Seismic and gravity constraints on the crust and uppermost mantle structure of the Cape Verde mid-plate swell, *Geophys. J. Int.*, *182*, 531–550, doi: 10.1111/j.1365-246X.04641x.

Ye, S., J. P. Canales, R. Rhim, J. J. Danobeitia, and J. Gallart (1999), A crustal transect through the northern and north-eastern part of the volcanic edifice of Gran Canaria, *J. Geodyn.*, *28*, 3–26.

Zucca, J. J., D. P. Hill, and R. L. Kovach (1982), Crustal structure of Mauna Loa Volcano, Hawaii, from seismic refraction and gravity data, *Bull. Seismol. Sco. Am.*, *72*, 1535–1550.